

**PHS PUBLIC ACCESS**

Author manuscript

*Stem Cells*. Author manuscript; available in PMC 2017 June 01.

Published in final edited form as:

*Stem Cells*. 2016 June ; 34(6): 1553–1562. doi:10.1002/stem.2356.**Stepwise Differentiation of Retinal Ganglion Cells from Human Pluripotent Stem Cells Enables Analysis of Glaucomatous Neurodegeneration****Sarah K. Ohlemacher<sup>1</sup>, Akshayalakshmi Sridhar<sup>1</sup>, Yucheng Xiao<sup>2</sup>, Alexandra E. Hochstetler<sup>1</sup>, Mansoor Sarfarazi<sup>3</sup>, Theodore R. Cummins<sup>2,4</sup>, and Jason S. Meyer<sup>1,2,5,\*</sup>**<sup>1</sup>Department of Biology, Indiana University Purdue University Indianapolis, Indianapolis IN 46202.<sup>2</sup>Stark Neurosciences Research Institute, Indiana University, Indianapolis IN 46202.<sup>3</sup>Molecular Ophthalmic Genetics Laboratory, University of Connecticut Health Center, Farmington CT 06030.<sup>4</sup>Department of Pharmacology and Toxicology, Indiana University, Indianapolis IN 46202.<sup>5</sup>Department of Medical and Molecular Genetics, Indiana University, Indianapolis IN 46202.**Abstract**

Human pluripotent stem cells (hPSCs), including both embryonic and induced pluripotent stem cells, possess the unique ability to readily differentiate into any cell type of the body, including cells of the retina. Although previous studies have demonstrated the ability to differentiate hPSCs to a retinal lineage, the ability to derive retinal ganglion cells (RGCs) from hPSCs has been complicated by the lack of specific markers with which to identify these cells from a pluripotent source. In the current study, the definitive identification of hPSC-derived RGCs was accomplished by their directed, stepwise differentiation through an enriched retinal progenitor intermediary, with resultant RGCs expressing a full complement of associated features and proper functional characteristics. These results served as the basis for the establishment of induced pluripotent stem cells (iPSCs) from a patient with a genetically inherited form of glaucoma, which results in damage and loss of RGCs. Patient-derived RGCs specifically exhibited a dramatic increase in apoptosis, similar to the targeted loss of RGCs in glaucoma, which was significantly rescued by the addition of candidate neuroprotective factors. Thus, the current study serves to establish a method by which to definitively acquire and identify RGCs from hPSCs and demonstrates the

\*To whom correspondence should be addressed: Jason S. Meyer, PhD, 723 West Michigan Street, SL306, Indiana University Purdue University Indianapolis, Indianapolis IN 46202, (317) 274-1040, ; Email: meyerjas@iupui.edu

**Author Contributions:**

Sarah Ohlemacher: Conception and design, financial support, collection and/or assembly of data, data analysis and interpretation, manuscript writing, final approval of manuscript

Akshayalakshmi Sridhar: Conception and design, collection and/or assembly of data, data analysis and interpretation

Yucheng Xiao: Collection and/or assembly of data, data analysis and interpretation

Alexandra Hochstetler: Collection and/or assembly of data

Mansoor Sarfarazi: Conception and design, Provision of study material or patients

Theodore Cummins: Conception and design, financial support, data analysis and interpretation, manuscript writing

Jason Meyer: Conception and design, financial support, collection and/or assembly of data, data analysis and interpretation, manuscript writing, final approval of manuscript

**Disclosures:** The authors have no competing interests to disclose.

ability of hPSCs to serve as an effective in vitro model of disease progression. Moreover, iPSC-derived RGCs can be utilized for future drug screening approaches to identify targets for the treatment of glaucoma and other optic neuropathies.

## Keywords

Pluripotent stem cell; retina; differentiation; retinal ganglion cell; glaucoma

---

## Introduction

Human pluripotent stem cells (hPSCs) offer the unique and unprecedented ability to study the differentiation of specific cellular lineages, particularly at those stages of development that would otherwise be inaccessible to investigation. As such, they have been demonstrated to serve as powerful in vitro models for human ontogenesis<sup>1,2</sup>. When derived from specific patient populations, human induced pluripotent stem cells (iPSCs) are capable of serving as in vitro models of disease progression<sup>3,8</sup>, effectively bridging the gap between basic and translational research. Among the diseases that may be effectively modeled with iPSCs, those affecting the retina have been of particular interest<sup>4,5,9,11</sup> as a number of methods exist to derive all of the major cell types of the retina<sup>4,12,20</sup>, and a relative lack of effective treatments and cures exist for many blinding disorders.

While many previous studies have focused upon the ability to derive and utilize retinal cells such as photoreceptors and retinal pigment epithelium<sup>4,5,12,21</sup>, retinal ganglion cells (RGCs) have been largely overlooked to date. As the projection neurons of the retina, RGCs effectively serve as the connection between the eye and the brain. Furthermore, RGCs are the predominant affected cell type in a group of diseases known as optic neuropathies, the most common of which is glaucoma with a current incidence of over 60 million individuals worldwide<sup>22,23</sup>. Within the context of the retina, RGCs are often identified by the expression of a limited set of markers that are specific to these cells. However, when derived from a pluripotent cell source, these markers are no longer specific for RGCs as they are expressed elsewhere in the nervous system. To date, the detailed description and utilization of hPSC-derived RGCs has been largely lacking likely due to the shortage of reliable markers with which to definitively identify these cells without the assurance of a retinal lineage, although previous studies have demonstrated the ability to derive cells with RGC-like characteristics<sup>4,12,14,18,24,28</sup>. Thus, a systematic, detailed analysis of these cells is warranted in order to serve as a comprehensive *in vitro* model of RGC development, as well as the application of patient-derived RGCs for disease modeling.

To this end, efforts were undertaken to comprehensively detail the differentiation of RGCs, with subsequent application of these approaches to a glaucoma patient-derived line of iPSCs. Lines of hPSCs were directed to differentiate in a stepwise fashion specifically toward a retinal lineage, and highly enriched populations of retinal progenitor cells were readily identified and isolated, yielding a highly purified population. Upon further differentiation of these retinal progenitor cells, presumptive RGCs were identifiable within a total of 40 days of differentiation and were characterized for morphological, phenotypic, and

physiological features of native RGCs. These cells were found to express all of the observed features associated with RGCs and importantly, the possibility was excluded to have differentiated into alternate lineages bearing similar phenotypic markers. Furthermore, hPSC-derived cells possessed expected physiological properties of RGCs<sup>29</sup>. Following the conclusive identification and characterization of hPSC-derived RGCs, similar approaches were undertaken for iPSCs derived from a glaucoma patient possessing an E50K mutation in the Optineurin (OPTN) gene, responsible for some familial forms of glaucoma<sup>30,36</sup>. These cells were differentiated to an RGC fate, at which point their ability to serve as an *in vitro* model for studies of disease progression and drug screening were tested. The results of these studies support a role for hPSCs as an effective *in vitro* model for human RGC development and functionality, as well as for use in studies of cellular mechanisms underlying disease progression in optic neuropathies.

## Materials and Methods

### Maintenance of hPSCs

hPSCs were maintained as previously described<sup>15,17</sup>. Briefly, three lines of control human pluripotent stem cells (H9, H7<sup>37</sup> and miPS2<sup>38</sup>) were used, and three lines of patient-derived induced pluripotent stem cells from an OPTN E50K patient were derived. All cell lines were maintained in the pluripotent state with mTeSR1 medium (Stemcell Technologies) on matrigel-coated 6-well plates. Cells were passaged upon reaching confluency of approximately 70%. Areas of spontaneous differentiation were initially identified by their distinct appearance and were mechanically removed. Colonies of hPSCs were then enzymatically lifted with dispase (2 mg/ml) for approximately 15 minutes and passaged at a ratio of 1:6 onto freshly-coated matrigel plates in mTeSR1 medium. Passaging of hPSCs typically occurred every 4-5 days.

### Differentiation of hPSCs

Differentiation of hPSCs to a retinal lineage was performed with modifications to previously established protocols<sup>15</sup>. Briefly, embryoid bodies (EBs) were generated from undifferentiated colonies of hPSCs by lifting adherent cultures with dispase. EBs were gradually transitioned into Neural Induction Medium (NIM) consisting of DMEM/F12 (1:1), N2 supplement, MEM nonessential amino acids and heparin (2 µg/ml). After a total of 7 days of differentiation, EBs were plated onto uncoated 6-well plates and induced to adhere by the addition of 10% FBS overnight. The next day, NIM was replaced without FBS and medium was subsequently changed every other day until day 16. At this point, cells were lifted from plates by mechanical scraping or pipetting to dislodge colonies and generate neurospheres in suspension cultures. Neurospheres were maintained in Retinal Differentiation Medium (RDM) consisting of DMEM/F12 (3:1), MEM non-essential amino acids, B27 supplement, and antibiotics. Medium was replenished every 2-3 days thereafter until the desired day of differentiation was reached. At this point, retinal neurospheres were isolated according to previously established protocols<sup>4,15,17,18,39</sup> based upon morphological cues exhibited by the neurospheres. As indicated in some experiments, OPTN iPSC-derived neurospheres were treated with either BDNF (100 ng/mL) or PEDF (100 ng/ml) from day 50 to day 70 of differentiation. Neurospheres were either harvested for RNA analysis, or

partially dissociated with accutase and plated onto poly-L-ornithine/laminin-coated coverslips for immunocytochemical analysis.

### Reprogramming of fibroblasts to iPSCs

The generation of OPTN glaucoma patient iPSCs was performed using mRNA reprogramming strategies as previously described<sup>40</sup>. Synthetic mRNAs with a microRNA booster kit (Stemgent) were introduced into OPTN fibroblasts through the use of Stemfect Transfection Reagent following manufacturers instructions. mRNAs were transfected daily for a total of 14 days. Within the first 20 days of reprogramming, some fibroblasts began to lose their elongated morphology and displayed the typical tightly packed morphology of iPSC cell colonies. Individual colonies of prospective iPSCs were identified, manually isolated, and clonally expanded to yield lines of patient-specific iPSCs. Newly established lines of iPSCs were maintained as described above.

### RT-PCR

RNA was isolated from retinal neurospheres using the Picopure RNA Isolation Kit (LifeTechnologies), with subsequent cDNA synthesis achieved utilizing the iScript cDNA synthesis kit (BioRad). PCR analysis was accomplished using Go-Taq PCR Master Mix (Promega), while qPCR analysis was performed with SybrGreen (Life Technologies). For RTPCR experiments, reactions were performed for 35 cycles and products were run on 2% agarose gels. Primers for RT-PCR and qRT-PCR analysis can be found in Supplemental Tables 1 and 2.

### Immunocytochemistry and Data Quantification

Samples were collected at indicated timepoints of differentiation and plated on poly-L-ornithine and laminin-coated coverslips. Cells were fixed in a 4% paraformaldehyde and phosphate buffer (PBS) solution for 30 minutes. Alternatively, neurospheres were processed for cryostat sectioning as indicated. For this purpose, neurospheres were fixed in 4% paraformaldehyde and PBS for 45 minutes and then introduced into a 20% sucrose solution in PBS for equilibration overnight at 4 degrees. The following day, sucrose solution was aspirated and changed to a 30% sucrose solution at 4°C. Following equilibration, neurospheres were embedded in OCT, frozen in dry ice and stored at -80°C until sectioning. Cryostat sections were cut at a thickness of 10 microns and stored at -80°C until use for immunocytochemistry.

For immunostaining of both coverslips and cryostat slides, samples were initially washed three times with PBS and permeabilized with 0.2% Triton X-100 for 10 minutes at room temperature. 10% donkey serum in PBS was used as a blocking agent for one hour at room temperature and primary antibodies (Supplemental Table 3) were applied in a solution consisting of 5% donkey serum and 0.1% Triton X-100 overnight at 4°C. The next day, samples were washed with PBS and 10% donkey serum blocking agent was applied for 10 minutes at room temperature. Samples were treated with secondary antibodies diluted in a 5% donkey serum and 0.1% Triton X-100 solution for one hour at room temperature, followed by 3 washes with PBS. Samples were mounted onto slides and cells were imaged

with either a Leica DM5500 fluorescence microscope or an Olympus Fluoview 2000 confocal microscope.

Quantification of cell counts was performed with Image-J software using immunostained samples. For each experimental condition, three different lines of hPSCs were utilized. Within these different cell lines, a minimum of three images were collected from at least three separate experiments performed at different passage number from each cell line. Each image was quantified to calculate the percentage of BRN3-positive cells, as well as the abundance of activated caspase-3 expression relative to the total number of BRN3-positive cells. ANOVA statistical analyses or student's t-tests were performed with Prism software (Graphpad) to determine statistically significant differences at a p-value of less than 0.05. Size of the Golgi complex was determined by GM130 staining similar to previous reports<sup>41,43</sup> by calculating the total area of GM130-positive staining utilizing ImageJ software, and then dividing this number by the total number of DAPI-positive nuclei. A minimum of three samples were analyzed per experiment to obtain the average Golgi area per cell. A student's t-test was used to determine statistical significance using Prism software, and significant differences were identified at a p value less than 0.05.

## Electrophysiology

Whole-cell patch-clamp recordings were carried out at room temperature (21°C) as previously described<sup>44</sup> using an EPC-10 amplifier and the Pulse8.31 program (HEKA, Lambrecht/Pfalz, Germany). Fire-polished electrodes were fabricated from borosilicate capillary glass (1.2-mm outer diameter, 0.69-mm inner diameter; Sutter Instrument Co., Novato, CA) using a P-97 puller (Sutter Instrument Co., Novato, CA). After filling with the intracellular solution containing (in mM): KCl 140, MgCl<sub>2</sub> 5, EGTA 5, CaCl<sub>2</sub> 2.5, Hepes 10, ATP 4, GTP 0.3, Phosphocreatine 8, pH7.3 (adjusted with KOH), the access resistance of electrode pipettes ranged between 4 and 5 MΩ. The bathing solution contained (in mM): NaCl 140, MgCl<sub>2</sub> 1, KCl 5, CaCl<sub>2</sub> 2, Hepes 10, Glucose 10, pH7.3 (adjusted with NaOH). After establishing the whole-cell recording configuration, cells were allowed to stabilize for 2-3 minutes in current-clamp mode before initiating ramp current injection to measure action potential activity. Cells were held at -100 mV to stabilize for 5 minutes in voltage-clamp mode before applying depolarizing voltage steps to measure potassium and sodium currents. A -P/4 subtraction protocol was used to remove linear leak current and capacitance artifact for all voltage clamp recordings. Voltage errors were minimized using more than 80% series resistance compensation. Membrane currents were filtered at 5 kHz and sampled at 20 kHz. Tetrodotoxin (TTX, 5 μM) and tetraethylammonium (TEA, 100 mM) stock solutions were made using the bathing solution. TTX or TEA was diluted into a 300 μl recording chamber to achieve the final concentration.

## Results

### Identification of hPSC-Derived Retinal Ganglion Cells

The definitive identification of RGCs from a pluripotent source has been complicated by the lack of specific markers to identify these cells. The expression of the transcription factor BRN3 has been widely utilized to identify cells with RGC-like characteristics<sup>4, 12, 14, 18, 24, 26</sup>.

However, when derived from hPSCs, such markers lose their specificity as BRN3 is also expressed in other cell types of the central nervous system, particularly hair cells of the auditory system<sup>45</sup> as well as somatosensory neurons<sup>46</sup>. Thus, to conclusively establish the RGC nature of these cells, their derivation and identification necessitates the detailed stepwise differentiation through early neural and retinal progenitor intermediaries.

To this end, initial efforts were focused upon the differentiation and definitive identification of hPSC-derived RGCs. As a starting point, hPSCs were directed to differentiate to an optic vesicle-like stage of retinogenesis as previously described<sup>4,15,17,18,25</sup>, at which point highly enriched populations of CHX10-positive retinal progenitor cells comprised  $50.02 \pm 1.95\%$  of all neurospheres. These retinal populations were readily identified and isolated apart from their non-retinal forebrain counterparts based upon morphological cues (Figure 1A-C), allowing for the subsequent classification of further differentiated phenotypes to the retinal lineage. Within 40 total days of differentiation, enriched populations of optic vesicle-like retinal neurospheres began to express BRN3 as well as a compliment of other retinal-associated transcription factors when analyzed by RT-PCR (Figure 1D). Conversely, no expression of genes characteristic of the auditory<sup>45</sup> and somatosensory<sup>46</sup> lineages was detected. Taken together, these results confirm the retinal phenotype associated with these BRN3-positive cells. Immunocytochemistry analysis further confirmed the expression of BRN3 with other markers of the retinal lineage (Figure 1E-G). Specifically, BRN3 expression was often found colocalized with markers typically associated with retinal progenitor cells and some RGCs such as PAX6 and SIX6. However, colocalization of BRN3 with markers indicative of other retinal cell types such as Recoverin was not observed (Figure S1).

The temporal birth order of specific retinal cell types has been well characterized in vivo, with retinal progenitors giving rise to RGCs and cone photoreceptors early while rods and Müller glia emerge later<sup>47,48</sup>. Through immunocytochemical analysis, early stages of this stepwise progression to an RGC fate could be observed (Figure 2A), with PAX6-positive neural progenitors the first stage in this differentiation process. Following the identification and isolation of retinal neurospheres, robust differentiation of CHX10-positive retinal progenitors was observed. The appearance of BRN3-expressing RGCs could be observed shortly thereafter, followed by the onset of recoverin-positive photoreceptor-like cells. RT-PCR analysis further confirmed this stepwise pattern of retinal fate determination (Figure 2B).

### Characterization and Functional Analysis of hPSC-Derived Retinal Ganglion Cells

The expression of BRN3, along with the differentiation of hPSCs through the stepwise process of retinal differentiation, aids in the identification of resultant RGCs. Overall, approximately  $36.1 \pm 1.7\%$  of cells expressed the RGC-associated transcription factor BRN3 within the first 40 days of differentiation (Figure 3A). Beyond the expression of BRN3, however, a variety of other features are associated with the development of RGCs. Upon differentiation, presumptive RGCs co-expressed a wide array of such factors associated with RGC specification (Figure 3B-E). Furthermore, maturation and morphological changes of these cells were readily observed, as BRN3-positive RGCs were found associated with

MAP2-positive neurite extensions (Figure 3F). Interestingly, a small population of melanopsin-expressing cells were observed, indicative of intrinsically photosensitive retinal ganglion cells (ipRGCs). These cells expressed high levels of melanopsin (Figure 3G) and largely lacked BRN3 expression (Figure 3G'), typical of the M1 class of ipRGCs<sup>49,51</sup>.

The ability to exhibit lengthy neurite outgrowths is a further characteristic of RGCs when compared to other neurons of the retina. Following prolonged growth *in vitro*, extensive neurite outgrowth was readily observed from BRN3-expressing RGCs (Figure 3H). Cytoskeletal components became compartmentalized with clear separation of MAP2 expression in somatodendritic regions and Tau expression confined to axonal extensions that fasciculated and extended over long distances. The progressive acquisition of RGC characteristics, as well as the differential expression of these characteristics apart from non-retinal forebrain cells, was further characterized by qRT-PCR analysis (Figure 3I-J). In comparison to retinal progenitor cells identified at earlier stages of differentiation, RGC populations exhibited a robust increase in the expression of RGC-associated genes, along with a significant decrease in the expression of retinal progenitor-associated genes (Figure 3I). Furthermore, when compared to age-matched non-retinal forebrain populations as indicated above (Figure 1A), a significant increase was observed in the expression of retinal and RGC-associated genes (Figure 3J).

As projection neurons connecting the eye with the brain, and unlike most other neurons of the retina, RGCs transmit visual information via elicitation of action potentials through the use of voltage-gated ion channels<sup>29</sup>. To confirm whether hPSC-derived RGCs are capable of similar physiological activity, prospective RGCs were first morphologically identified for electrophysiological analysis based upon extensive neurite outgrowth (Figure 4A) typical of these cells<sup>15,52,53</sup>. Electrophysiological activity of hPSC-derived RGCs was then analyzed by patch clamp analysis, and recorded cells were filled with Lucifer Yellow for subsequent immunocytochemical analysis for BRN3 expression to definitively identify analyzed cells as RGCs (Figure 4B). hPSC-derived RGCs demonstrated the ability to fire action potentials (Figure 4C) and exhibited a hyperpolarized resting membrane potential (Figure 4D). These electrophysiological properties were associated with ionic currents, including outward flow that could be blocked by the addition of TEA, indicating the presence of voltage-gated K<sup>+</sup> channels (Figure 4E), as well as inward current flow that was sensitive to the voltage-gated Na<sup>+</sup> channel blocker TTX (Figure 4F). Furthermore, both K<sup>+</sup> and Na<sup>+</sup> ionic currents were shown to be voltage-dependent in nature.

### **In Vitro Modeling of Optic Neuropathies Using Patient Specific iPSCs**

The ability to derive RGCs from an hPSC source has important implications beyond studies of developmental biology<sup>1,2</sup>, including translational applications<sup>3,5,7</sup> such as *in vitro* disease modeling and pharmacological screening<sup>54,56</sup> when derived from specific patient sources. Mutations in the OPTN gene have been extensively documented to result in severe RGC degeneration associated with primary open angle glaucoma<sup>30,35</sup> and therefore, should provide an effective *in vitro* tool for studies of underlying disease mechanisms, as well as subsequent pharmacological screening. To this end, skin fibroblasts from a patient possessing an E50K missense mutation in the OPTN gene were reprogrammed to

pluripotency, exhibiting robust expression of a full complement of pluripotency-associated factors (Figure S2) and the ability to give rise to cell types of all three germ layers (Figure S3).

Upon differentiation, enriched populations of OPTN iPSC-derived retinal neurospheres (Figure 5A) were characterized by robust expression of CHX10 (Figure 5B), indicative of a retinal progenitor state<sup>4,39,57</sup>. Subsequent differentiation of these retinal progenitors yielded BRN3-positive cells that could be definitively identified as RGCs due to their retinal lineage. These RGCs exhibited elaborate MAP2-positive neuronal morphologies and formation of complex neural networks (Figure 5C-D). Undifferentiated OPTN iPSCs exhibited a disorganized Golgi morphology that led to a significant increase in size (Figure S4A-C), as previously reported<sup>32,33,42</sup>. Interestingly, however, differentiation to the affected RGC phenotype yielded no significant difference in the size and organization of the Golgi of OPTN RGCs compared to control RGCs (Figure S4D-F).

To further examine the applicability of OPTN iPSC-derived RGCs as an *in vitro* model for glaucoma, the activation of caspase-3 was analyzed and quantified via immunocytochemistry in comparison to unaffected control lines. In undifferentiated cultures, little activation of caspase-3 was observed and no significant differences were seen between control and OPTN iPSCs (Figure 5E-G). Upon differentiation of these cells to the affected RGC cell type, caspase-3 activation was minimal in control iPSC-derived RGCs but was significantly increased in OPTN iPSC-derived RGCs (Figure 5H-J). Given these increased levels of apoptosis, the ability of these cells to serve as a tool for pharmacological screening was subsequently tested, utilizing factors previously identified as neuroprotective in other systems<sup>58,63</sup>. Upon treatment of OPTN iPSC-derived RGCs with either BDNF or PEDF, a significant reduction in caspase-3 activation was observed (Figure 5K-M).

## Discussion

The results presented here demonstrate the robust derivation and definitive identification of RGCs from hPSCs as identified by the combination of morphological, phenotypic, and physiological measures. Furthermore, these efforts were applied to establish an *in vitro* model of glaucoma with patient-derived iPSCs, allowing for the ability to study associated underlying features of the disease itself, as well as the potential use as a tool for pharmacological screening<sup>54</sup>.

Although previous reports have demonstrated that hPSCs can acquire retinal characteristics upon differentiation<sup>4,12,20,25</sup>, including features of retinal ganglion cells<sup>4,12,18,24,28</sup>, many markers used to identify RGCs, particularly BRN3, are also expressed in other neural cells, including some auditory neurons<sup>45</sup> as well as somatosensory neurons<sup>46</sup>. Thus, efforts to unequivocally assign an RGC identity are complicated without thorough and systematic characterization. Moreover, BRN3 exists in three different forms, namely BRN3A, BRN3B, and BRN3C<sup>64,65</sup>. While the current studies analyzed the overall expression of BRN3, it is likely that most of the cells expressed BRN3B, as this form is known to play a critical role in the differentiation and survival of RGCs, and is also known to be expressed earlier in development than other forms of BRN3.



In the current study, multiple approaches were undertaken to ensure that presumptive RGCs had indeed adopted this fate. First, retinal differentiation proceeded through a retinal progenitor stage that could be readily identified and isolated, yielding highly enriched populations of CHX10-expressing retinal progenitor cells, with subsequent expression of BRN3 allowing for more definitive identification of RGCs. Additionally, BRN3 expression was often found expressed in close association with other retinal cell types, while expression of markers associated with auditory and somatosensory lineages was not observed. Thus, the data presented provides the strongest evidence to date of the ability to conclusively differentiate RGCs from hPSCs.

Intrinsically photosensitive retinal ganglion cells (ipRGCs) are a specific subtype of RGC that function in non-visual phototransduction processes including circadian entrainment and pupillary responses<sup>49,51</sup>. The data presented within the current study is the first to demonstrate the differentiation of ipRGCs from hPSCs, as detected by the expression of the phototransduction protein melanopsin. While the derivation of these cells was exceedingly rare, the presence of these cells allows for future investigation into the developmental specification of ipRGCs, as well as studies analyzing the damage and loss of ipRGCs in a variety of injuries and degenerative disorders of the retina<sup>66</sup>.

Beyond phenotypic features, these hPSC-derived RGCs also possessed appropriate morphological and physiological features. After prolonged growth *in vitro*, hPSC-derived RGCs were capable of extensive neurite outgrowth, which was specifically directed toward other aggregates of cells, perhaps due to paracrine signaling. Further maturation of hPSC-derived RGCs was also observed in the compartmentalization of MAP2 and Tau, cytoskeletal proteins that are found widely expressed in immature neurons but whose expression becomes confined to somatodendritic and axonal regions, respectively, in mature neurons<sup>67</sup>. Furthermore, these cells exhibited the ability to function physiologically, with the ability to conduct sodium and potassium through voltage-dependent channels as well as the ability to fire action potentials. Although these features are characteristic of many types of neurons<sup>29</sup>, in the retina these characteristics are specifically found within the RGCs as well as a subset of amacrine cells. While these cells exhibited a hyperpolarized resting membrane potential, this potential was recorded at an average of approximately  $-40$  mV, indicating that these cells have not yet reached a fully mature state. Future experiments will necessitate the development of methods by which these hPSC-derived RGCs can be induced to mature further *in vitro*.

Beyond the differentiation and characterization of hPSC-derived RGCs, efforts were also focused on the development of iPSC-based models of optic neuropathies. Glaucoma is the most prevalent of the optic neuropathies, with a current incidence of more than 60 million individuals worldwide<sup>22,23</sup>. However, a variety of factors exist which are causative or at least associated with the onset of glaucomatous neurodegeneration<sup>68,69</sup>. Mutations in the OPTN gene were selected for study, particularly the E50K mutation which has been previously demonstrated to result in a particularly severe neurodegenerative phenotype<sup>30,32</sup>. While the results obtained with these cells will be of significance for future studies of this glaucoma-associated genotype, these results could also prove to be more profound for other glaucoma phenotypes as well. As other factors such as elevated intraocular pressure have been

suggested to serve as a trigger for subsequent degeneration of RGCs<sup>69</sup>, mutations in genes including OPTN could provide a similar trigger, with downstream effects mimicking features of glaucoma common to many underlying causes.

Whereas previous studies have analyzed features of glaucoma in RGCs by utilizing animal models or non-affected cell types *in vitro*<sup>42,70,71</sup>, the development of a human induced pluripotent stem cell model of glaucoma allows for precise analysis of the affected cell type. The ability to study features of the disease process in human cells from the affected cell type is of utmost importance, as some previous studies have identified disruptions in the Golgi complex as a hallmark of certain mutations in OPTN, including the E50K mutation<sup>32,33,42</sup>. While this phenotype was recapitulated in undifferentiated OPTN iPSCs, this Golgi fragmentation was not observed upon differentiation to RGCs, the cell type directly affected by the disease process. It is not completely surprising that the Golgi phenotype changed following differentiation, as previous studies have demonstrated that the shape and size of the Golgi complex can, and indeed often does, vary from one type of cell to another<sup>72,73</sup>. The size and shape of the Golgi complex are often larger in those cells that have greater intracellular trafficking demands, particularly those that are mitotically active such as undifferentiated hPSCs. This is reflected in the fact that the Golgi size was markedly larger in the undifferentiated state compared to differentiated RGCs, regardless of whether the cells were from control or E50K sources. Thus, there is not necessarily any reason to expect that differences between cell sources in the undifferentiated state will be maintained at later stages of differentiation. In fact, the data presented strongly suggests that differences in Golgi morphology do not likely contribute to increased caspase-3 activation observed in OPTN E50K cells. Thus, disruptions to the Golgi complex may not have any direct connection to the health and survival of RGCs and consequently, may not play a role in glaucomatous neurodegeneration observed in patient samples. Such a result underscores the importance of iPSC-based models of inherited diseases and the ability to differentiate these cells to the affected cell type. The increased apoptosis observed in OPTN cells appeared to be specific for RGCs, the affected cell type, as no significant differences were observed in undifferentiated OPTN iPSCs compared to control cell lines. As such, the development of this *in vitro* model of glaucoma will allow for future studies analyzing precise mechanisms underlying glaucomatous neurodegeneration. The results of these studies also highlight the potential of iPSCs to serve as a tool for pharmacological screening<sup>54,56</sup>, as treatment of OPTN iPSC-derived RGCs with either BDNF or PEDF was able to partially rescue these cells from apoptosis. Interestingly, treatment with these neuroprotective factors yielded similar levels of cell survival. While the reason for this similarity is not known, the possibility exists for overlap in these two signaling pathways. While both BDNF and PEDF are known to inhibit the apoptotic pathway<sup>59,61,63</sup>, they also affect transcription through MEK/ERK signaling pathways<sup>58</sup>. Thus, the similar net effects produced by BDNF and PEDF could be due to convergence of these signaling pathways within the cell.

## Conclusion

Taken together, the results of the current study represent the most comprehensive description of RGC derivation from an hPSC source by morphological, phenotypic, and functional parameters, as well as the ability to utilize these approaches for studies of optic neuropathies

such as glaucoma. On a broader level, this study establishes the suitability of hPSCs to analyze critical stages of RGC development from a human source. Furthermore, these results demonstrate the applicability of hPSC-derived RGCs for disease modeling and pharmacological screening for a host of optic neuropathies, both complementing existing animal models as well as narrowing the gap to clinical applications.

## Supplementary Material

Refer to Web version on PubMed Central for supplementary material.

## Acknowledgments

We thank B. Hamilton for assistance with reprogramming of OPTN fibroblasts. Grant support provided by NIH grant R01 EY024984 (JSM), R01 NS053422 (TRC), BrightFocus foundation grant number G201027 (JSM), a Research Support Funds Grant from the Office of the Vice Chancellor for Research at IUPUI (JSM), a training grant within the ICTSI NIH/NCRR Grant Number TL1TR001107 (SKO) and a Project Development Team award within the ICTSI NIH/NCRR Grant Number UL1TR001108 (JSM).

## References

1. Keller G. Embryonic stem cell differentiation: emergence of a new era in biology and medicine. *Genes & development*. 2005; 19:1129–1155. [PubMed: 15905405]
2. Pera MF, Trounson AO. Human embryonic stem cells: prospects for development. *Development* (Cambridge, England). 2004; 131:5515–5525.
3. Marchetto MC, Brennand KJ, Boyer LF, et al. Induced pluripotent stem cells (iPSCs) and neurological disease modeling: progress and promises. *Human molecular genetics*. 2011; 20:R109–115. [PubMed: 21828073]
4. Meyer JS, Howden SE, Wallace KA, et al. Optic vesicle-like structures derived from human pluripotent stem cells facilitate a customized approach to retinal disease treatment. *Stem cells* (Dayton, Ohio). 2011; 29:1206–1218.
5. Singh R, Shen W, Kuai D, et al. iPSC cell modeling of Best disease: insights into the pathophysiology of an inherited macular degeneration. *Human molecular genetics*. 2013; 22:593–607. [PubMed: 23139242]
6. Brennand KJ, Simone A, Tran N, et al. Modeling psychiatric disorders at the cellular and network levels. *Molecular psychiatry*. 2012; 17:1239–1253. [PubMed: 22472874]
7. Mattis VB, Tom C, Akimov S, et al. HD iPSC-derived neural progenitors accumulate in culture and are susceptible to BDNF withdrawal due to glutamate toxicity. *Human molecular genetics*. 2015; 24:3257–3271. [PubMed: 25740845]
8. Yoshida T, Ozawa Y, Suzuki K, et al. The use of induced pluripotent stem cells to reveal pathogenic gene mutations and explore treatments for retinitis pigmentosa. *Molecular brain*. 2014; 7:45. [PubMed: 24935155]
9. Jin ZB, Okamoto S, Osakada F, et al. Modeling retinal degeneration using patient-specific induced pluripotent stem cells. *PloS one*. 2011; 6:e17084. [PubMed: 21347327]
10. Schwarz N, Carr AJ, Lane A, et al. Translational read-through of the RP2 Arg120stop mutation in patient iPSC-derived retinal pigment epithelium cells. *Human molecular genetics*. 2015; 24:972–986. [PubMed: 25292197]
11. Burnight ER, Wiley LA, Drack AV, et al. CEP290 gene transfer rescues Leber congenital amaurosis cellular phenotype. *Gene therapy*. 2014; 21:662–672. [PubMed: 24807808]
12. Lamba DA, McUsic A, Hirata RK, et al. Generation, purification and transplantation of photoreceptors derived from human induced pluripotent stem cells. *PloS one*. 2010; 5:e8763. [PubMed: 20098701]

13. Meyer JS, Shearer RL, Capowski EE, et al. Modeling early retinal development with human embryonic and induced pluripotent stem cells. *Proceedings of the National Academy of Sciences of the United States of America*. 2009; 106:16698–16703. [PubMed: 19706890]
14. Nakano T, Ando S, Takata N, et al. Self-formation of optic cups and storable stratified neural retina from human ESCs. *Cell stem cell*. 2012; 10:771–785. [PubMed: 22704518]
15. Ohlemacher SK, Iglesias CL, Sridhar A, et al. Generation of highly enriched populations of optic vesicle-like retinal cells from human pluripotent stem cells. *Current protocols in stem cell biology*. 2015; 32:1h.8.1–1h.8.20.
16. Osakada F, Ikeda H, Mandai M, et al. Toward the generation of rod and cone photoreceptors from mouse, monkey and human embryonic stem cells. *Nature biotechnology*. 2008; 26:215–224.
17. Sridhar A, Steward MM, Meyer JS. Nonxenogeneic growth and retinal differentiation of human induced pluripotent stem cells. *Stem cells translational medicine*. 2013; 2:255–264. [PubMed: 23512959]
18. Zhong X, Gutierrez C, Xue T, et al. Generation of three-dimensional retinal tissue with functional photoreceptors from human iPSCs. *Nature communications*. 2014; 5:4047.
19. Lamba DA, Karl MO, Ware CB, et al. Efficient generation of retinal progenitor cells from human embryonic stem cells. *Proceedings of the National Academy of Sciences of the United States of America*. 2006; 103:12769–12774. [PubMed: 16908856]
20. Mellough CB, Sernagor E, Moreno-Gimeno I, et al. Efficient stage-specific differentiation of human pluripotent stem cells toward retinal photoreceptor cells. *Stem cells (Dayton, Ohio)*. 2012; 30:673–686.
21. Boucherie C, Mukherjee S, Henckaerts E, et al. Brief report: self-organizing neuroepithelium from human pluripotent stem cells facilitates derivation of photoreceptors. *Stem cells (Dayton, Ohio)*. 2013; 31:408–414.
22. Tham YC, Li X, Wong TY, et al. Global prevalence of glaucoma and projections of glaucoma burden through 2040: a systematic review and meta-analysis. *Ophthalmology*. 2014; 121:2081–2090. [PubMed: 24974815]
23. Cedrone C, Mancino R, Cerulli A, et al. Epidemiology of primary glaucoma: prevalence, incidence, and blinding effects. *Progress in brain research*. 2008; 173:3–14. [PubMed: 18929097]
24. Maekawa Y, Onishi A, Matsushita K, et al. Optimized Culture System to Induce Neurite Outgrowth From Retinal Ganglion Cells in Three-Dimensional Retinal Aggregates Differentiated From Mouse and Human Embryonic Stem Cells. *Current eye research*. 2015:1–11.
25. Phillips MJ, Wallace KA, Dickerson SJ, et al. Blood-derived human iPS cells generate optic vesicle-like structures with the capacity to form retinal laminae and develop synapses. *Investigative ophthalmology & visual science*. 2012; 53:2007–2019. [PubMed: 22410558]
26. Riazifar H, Jia Y, Chen J, et al. Chemically induced specification of retinal ganglion cells from human embryonic and induced pluripotent stem cells. *Stem cells translational medicine*. 2014; 3:424–432. [PubMed: 24493857]
27. Tanaka T, Yokoi T, Tamalu F, et al. Generation of retinal ganglion cells with functional axons from human induced pluripotent stem cells. *Scientific reports*. 2015; 5:8344. [PubMed: 25666360]
28. Tucker BA, Solivan-Timpe F, Roos BR, et al. Duplication of TBK1 Stimulates Autophagy in iPSC-derived Retinal Cells from a Patient with Normal Tension Glaucoma. *Journal of stem cell research & therapy*. 2014; 3:161. [PubMed: 24883232]
29. Velte TJ, Masland RH. Action potentials in the dendrites of retinal ganglion cells. *Journal of neurophysiology*. 1999; 81:1412–1417. [PubMed: 10085366]
30. Allingham RR, Liu Y, Rhee DJ. The genetics of primary open-angle glaucoma: a review. *Experimental eye research*. 2009; 88:837–844. [PubMed: 19061886]
31. Fingert JH. Primary open-angle glaucoma genes. *Eye (London, England)*. 2011; 25:587–595.
32. Sarfarazi M, Rezaie T. Optineurin in primary open angle glaucoma. *Ophthalmology clinics of North America*. 2003; 16:529–541. [PubMed: 14740994]
33. Rezaie T, Child A, Hitchings R, et al. Adult-onset primary open-angle glaucoma caused by mutations in optineurin. *Science (New York, N.Y.)*. 2002; 295:1077–1079.

34. Minegishi Y, Iejima D, Kobayashi H, et al. Enhanced optineurin E50K-TBK1 interaction evokes protein insolubility and initiates familial primary open-angle glaucoma. *Human molecular genetics*. 2013; 22:3559–3567. [PubMed: 23669351]
35. Sarfarazi M, Stoilov I, Schenkman JB. Genetics and biochemistry of primary congenital glaucoma. *Ophthalmology clinics of North America*. 2003; 16:543–554, vi. [PubMed: 14740995]
36. Ying H, Yue BY. Cellular and molecular biology of optineurin. *International review of cell and molecular biology*. 2012; 294:223–258. [PubMed: 22364875]
37. Thomson JA, Itskovitz-Eldor J, Shapiro SS, et al. Embryonic stem cell lines derived from human blastocysts. *Science (New York, N.Y.)*. 1998; 282:1145–1147.
38. Sridhar A, Ohlemacher SK, Langer KB, et al. Robust Differentiation of mRNA-Reprogrammed Human Induced Pluripotent Stem Cells Toward a Retinal Lineage. *Stem cells translational medicine*. 2016
39. Phillips MJ, Perez ET, Martin JM, et al. Modeling human retinal development with patient-specific induced pluripotent stem cells reveals multiple roles for visual system homeobox 2. *Stem cells (Dayton, Ohio)*. 2014; 32:1480–1492.
40. Warren L, Manos PD, Ahfeldt T, et al. Highly efficient reprogramming to pluripotency and directed differentiation of human cells with synthetic modified mRNA. *Cell stem cell*. 2010; 7:618–630. [PubMed: 20888316]
41. Park BC, Shen X, Samaraweera M, et al. Studies of optineurin, a glaucoma gene: Golgi fragmentation and cell death from overexpression of wild-type and mutant optineurin in two ocular cell types. *The American journal of pathology*. 2006; 169:1976–1989. [PubMed: 17148662]
42. Turturro S, Shen X, Shyam R, et al. Effects of mutations and deletions in the human optineurin gene. *SpringerPlus*. 2014; 3:99. [PubMed: 24683533]
43. Ying H, Shen X, Park B, et al. Posttranslational modifications, localization, and protein interactions of optineurin, the product of a glaucoma gene. *PLoS one*. 2010; 5:e9168. [PubMed: 20161783]
44. Rowe AH, Xiao Y, Rowe MP, et al. Voltage-gated sodium channel in grasshopper mice defends against bark scorpion toxin. *Science (New York, N.Y.)*. 2013; 342:441–446.
45. Koehler KR, Mikosz AM, Molosh AI, et al. Generation of inner ear sensory epithelia from pluripotent stem cells in 3D culture. *Nature*. 2013; 500:217–221. [PubMed: 23842490]
46. Chambers SM, Qi Y, Mica Y, et al. Combined small-molecule inhibition accelerates developmental timing and converts human pluripotent stem cells into nociceptors. *Nature biotechnology*. 2012; 30:715–720.
47. Finlay BL. The developing and evolving retina: using time to organize form. *Brain research*. 2008; 1192:5–16. [PubMed: 17692298]
48. Livesey FJ, Cepko CL. Vertebrate neural cell-fate determination: lessons from the retina. *Nature reviews. Neuroscience*. 2001; 2:109–118. [PubMed: 11252990]
49. Rollag MD, Berson DM, Provencio I. Melanopsin, ganglion-cell photoreceptors, and mammalian photoentrainment. *Journal of biological rhythms*. 2003; 18:227–234. [PubMed: 12828280]
50. Lucas RJ, Peirson SN, Berson DM, et al. Measuring and using light in the melanopsin age. *Trends in neurosciences*. 2014; 37:1–9. [PubMed: 24287308]
51. Sand A, Schmidt TM, Kofuji P. Diverse types of ganglion cell photoreceptors in the mammalian retina. *Progress in retinal and eye research*. 2012; 31:287–302. [PubMed: 22480975]
52. Erskine L, Herrera E. The retinal ganglion cell axon's journey: insights into molecular mechanisms of axon guidance. *Developmental biology*. 2007; 308:1–14. [PubMed: 17560562]
53. Erskine L, Herrera E. Connecting the retina to the brain. *ASN neuro*. 2014;6.
54. Egawa N, Kitaoka S, Tsukita K, et al. Drug screening for ALS using patient-specific induced pluripotent stem cells. *Science translational medicine*. 2012; 4:145ra104.
55. Corti S, Faravelli I, Cardano M, et al. Human pluripotent stem cells as tools for neurodegenerative and neurodevelopmental disease modeling and drug discovery. *Expert opinion on drug discovery*. 2015; 10:615–629. [PubMed: 25891144]
56. Ko HC, Gelb BD. Concise review: drug discovery in the age of the induced pluripotent stem cell. *Stem cells translational medicine*. 2014; 3:500–509. [PubMed: 24493856]

57. Horsford DJ, Nguyen MT, Sellar GC, et al. Chx10 repression of Mitf is required for the maintenance of mammalian neuroretinal identity. *Development (Cambridge, England)*. 2005; 132:177–187.
58. Almeida RD, Manadas BJ, Melo CV, et al. Neuroprotection by BDNF against glutamate-induced apoptotic cell death is mediated by ERK and PI3-kinase pathways. *Cell death and differentiation*. 2005; 12:1329–1343. [PubMed: 15905876]
59. Vigneswara V, Berry M, Logan A, et al. Pigment epithelium-derived factor is retinal ganglion cell neuroprotective and axogenic after optic nerve crush injury. *Investigative ophthalmology & visual science*. 2013; 54:2624–2633. [PubMed: 23513062]
60. Alsina B, Vu T, Cohen-Cory S. Visualizing synapse formation in arborizing optic axons in vivo: dynamics and modulation by BDNF. *Nature neuroscience*. 2001; 4:1093–1101. [PubMed: 11593233]
61. Hu Y, Cho S, Goldberg JL. Neurotrophic effect of a novel TrkB agonist on retinal ganglion cells. *Investigative ophthalmology & visual science*. 2010; 51:1747–1754. [PubMed: 19875669]
62. Pang IH, Zeng H, Fleenor DL, et al. Pigment epithelium-derived factor protects retinal ganglion cells. *BMC neuroscience*. 2007; 8:11. [PubMed: 17261189]
63. Tombran-Tink J, Barnstable CJ. Therapeutic prospects for PEDF: more than a promising angiogenesis inhibitor. *Trends in molecular medicine*. 2003; 9:244–250. [PubMed: 12829012]
64. Badea TC, Nathans J. Morphologies of mouse retinal ganglion cells expressing transcription factors Brn3a, Brn3b, and Brn3c: analysis of wild type and mutant cells using genetically-directed sparse labeling. *Vision research*. 2011; 51:269–279. [PubMed: 20826176]
65. Nadal-Nicolas FM, Jimenez-Lopez M, Salinas-Navarro M, et al. Whole number, distribution and co-expression of brn3 transcription factors in retinal ganglion cells of adult albino and pigmented rats. *PloS one*. 2012; 7:e49830. [PubMed: 23166779]
66. Esquivia G, Lax P, Cuenca N. Impairment of intrinsically photosensitive retinal ganglion cells associated with late stages of retinal degeneration. *Investigative ophthalmology & visual science*. 2013; 54:4605–4618. [PubMed: 23766478]
67. Hirokawa N, Funakoshi T, Sato-Harada R, et al. Selective stabilization of tau in axons and microtubule-associated protein 2C in cell bodies and dendrites contributes to polarized localization of cytoskeletal proteins in mature neurons. *The Journal of cell biology*. 1996; 132:667–679. [PubMed: 8647897]
68. Qu J, Wang D, Grosskreutz CL. Mechanisms of retinal ganglion cell injury and defense in glaucoma. *Experimental eye research*. 2010; 91:48–53. [PubMed: 20394744]
69. Bagga H, Liu JH, Weinreb RN. Intraocular pressure measurements throughout the 24 h. *Current opinion in ophthalmology*. 2009; 20:79–83. [PubMed: 19240539]
70. Chi ZL, Akahori M, Obazawa M, et al. Overexpression of optineurin E50K disrupts Rab8 interaction and leads to a progressive retinal degeneration in mice. *Human molecular genetics*. 2010; 19:2606–2615. [PubMed: 20388642]
71. Tseng HC, Riday TT, McKee C, et al. Visual impairment in an optineurin mouse model of primary open-angle glaucoma. *Neurobiology of aging*. 2015; 36:2201–2212. [PubMed: 25818176]
72. Sengupta D, Linstedt AD. Control of organelle size: the Golgi complex. *Annual review of cell and developmental biology*. 2011; 27:57–77.
73. Shorter J, Warren G. Golgi architecture and inheritance. *Annual review of cell and developmental biology*. 2002; 18:379–420.

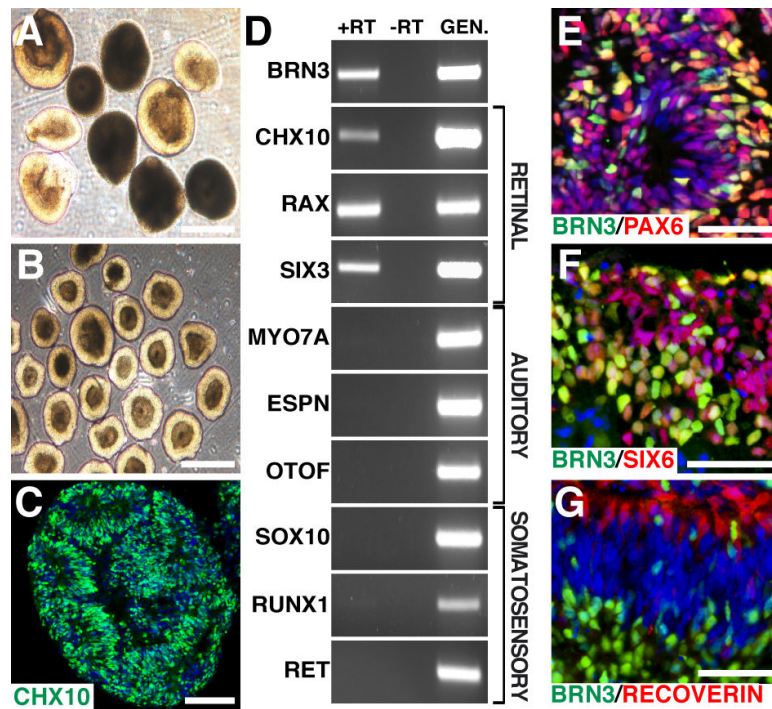


**Fig 1.**

Definitive identification of presumptive RGCs using BRN3 expression in differentiated cultures of hPSCs. After 25 days of differentiation, two morphologically distinct populations of neurospheres were observed (A), from which optic vesicle-like neurospheres were identified and isolated based upon their phase-bright appearance (B). Isolated optic vesicle neurospheres were highly enriched for CHX10-expressing retinal progenitor cells (C). After a total of 40 days of differentiation, RT-PCR analysis demonstrated that presumptive RGCs expressed BRN3 in conjunction with other retinal markers, but not markers of other BRN3-expressing lineages (D). Genomic DNA (Gen.) served as a positive control for RT-PCR experiments. Immunocytochemical analysis confirmed expression of BRN3 localized with other retinal markers (E-G). Images were captured at timepoints of 30 days of differentiation in A-C, 50 days of differentiation in E-F, and 70 days of differentiation in G. Scale bars equal 500  $\mu$ m in A-B, 100  $\mu$ m in C, and 50  $\mu$ m in D-F.

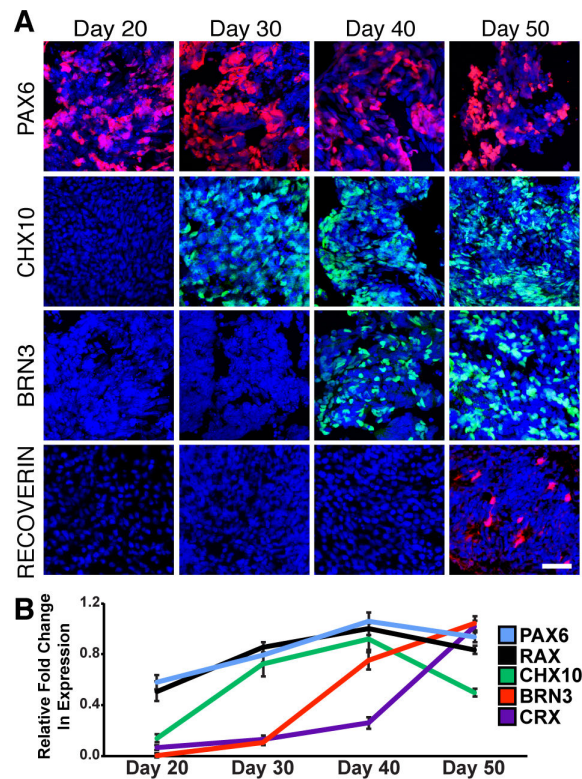


**Fig 2.** hPSC-derived RGCs are generated in a temporally appropriate sequence. Immunocytochemistry analysis revealed that BRN3-positive RGCs appeared subsequent to the establishment of neural (PAX6) and retinal (CHX10) progenitor fates, but prior to the generation of photoreceptor-like (Recoverin) cells (**A**). qRT-PCR analysis confirmed that genes associated with retinal and RGC development were expressed at developmentally-appropriate timepoints, with those genes associated with retinal progenitors expressed prior to the onset of RGC-specific genes (**B**). Scale bar equals 50  $\mu$ m.



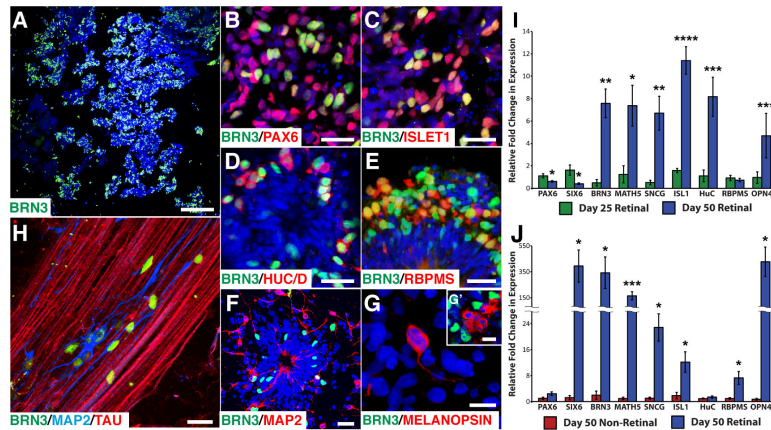


**Fig 3.** Phenotypic characterization of hPSC-derived RGCs. After 40 days of differentiation, BRN3-positive RGCs comprised approximately  $36.1 \pm 1.7\%$  of the total differentiated population (A). BRN3-positive RGCs expressed numerous RGC-associated markers (B-E), and began to extend MAP2-positive neurites (F) within a total of 50-70 days of differentiation. A small subset of intrinsically photosensitive melanopsin-positive RGCs were observed that were BRN3-negative (G-G') by 70 days of differentiation. Prolonged differentiation of hPSC-derived RGCs eventually gave rise to elaborate RGC-like morphologies exhibiting compartmentalized expression of MAP2 and TAU, including fasciculated TAU-positive axons (H) within 100 total days of differentiation. qRT-PCR analysis revealed that BRN3-expressing cultures exhibited significantly increased expression of RGC-associated transcripts compared to their retinal progenitor precursors (I), as well as their age-matched non-retinal forebrain counterparts (J). Significant differences indicated as \* =  $p < 0.05$ , \*\* =  $p < 0.01$ , \*\*\* =  $p < 0.005$ , \*\*\*\* =  $p < 0.001$ . Scale bars equal 200  $\mu\text{m}$  in A, 25  $\mu\text{m}$  in B-F, and 10  $\mu\text{m}$  in G-H.

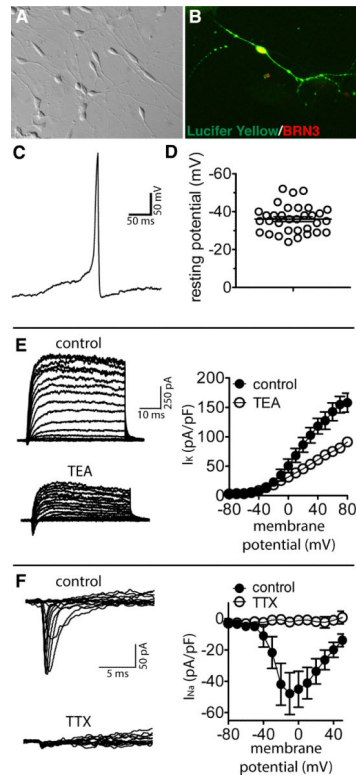


**Fig 4.**

Physiological analysis of hPSC-derived RGCs. Patch clamp analysis was performed and retinal ganglion cell morphologies were highlighted by DIC microscopy, including long neurite outgrowth in RGCs derived between 80-90 total days of differentiation (A). Recorded cells were filled with Lucifer Yellow for subsequent immunocytochemical confirmation of their RGC identity (B). hPSC-derived RGCs demonstrated the ability to fire action potentials (C) and exhibited a hyperpolarized resting membrane potential (D). These features were associated with the conductance of potassium and sodium through voltage-gated channels, which could be blocked by the addition of either TEA (E) or TTX (F).

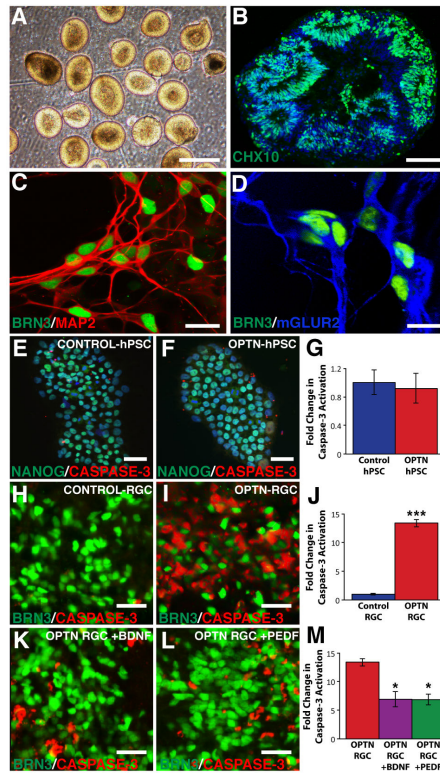


**Fig 5.** Patient-derived hPSCs can be utilized as an effective model of RGC neurodegeneration. Normal tension glaucoma patient fibroblasts, due to a mutation in the OPTN gene, were directed to differentiate to a retinal progenitor fate (A) as characterized by extensive expression of CHX10 (B) by a total of 30 days of differentiation. Retinal ganglion cells were subsequently differentiated and characterized by the expression of BRN3 as well as the development of complex neural networks, indicated by MAP2 (C) and mGluR2 (D) at 70 days of differentiation. In the pluripotent state, control and OPTN hPSCs exhibited no significant differences in apoptosis (E-G). Following differentiation for 70 days, OPTN RGCs demonstrated significantly increased apoptosis (H-J), which could be significantly reduced by treatment with select neuroprotective factors (K-M). Significant differences indicated as \* = p<0.05, \*\*\* = p<0.005. Scale bars equal 400 μm in A, 100 μm in B, 50 μm in C-F, and 25 μm in H-L.